

Poisson-random matrix transition in the QCD Dirac spectrum

Tamás G. Kovács

Institute for Nuclear Research of the Hungarian Academy of Sciences, Bem tér 18/c, H-4026 Debrecen, Hungary

Ferenc Pittler*

Department of Physics, University of Pécs, Ifjúság útja 6, H-7624 Pécs, Hungary

(Received 12 September 2012; published 28 December 2012)

At zero temperature the lowest part of the spectrum of the QCD Dirac operator is known to consist of delocalized modes that are described by random matrix statistics. In the present paper we show that the nature of these eigenmodes changes drastically when the system is driven through the finite temperature crossover. The lowest Dirac modes that are delocalized at low temperature become localized on the scale of the inverse temperature. At the same time the spectral statistics changes from random matrix to Poisson statistics. We demonstrate this with lattice QCD simulations using $2 + 1$ flavors of light dynamical quarks with physical masses. Drawing an analogy with Anderson transitions we also examine the mobility edge separating localized and delocalized modes in the spectrum. We show that it scales in the continuum limit and increases sharply with the temperature.

DOI: [10.1103/PhysRevD.86.114515](https://doi.org/10.1103/PhysRevD.86.114515)

PACS numbers: 12.38.Gc, 11.10.Wx, 11.30.Rd, 72.15.Rn

I. INTRODUCTION

The spectrum of the QCD quark Dirac operator is a quantity not directly accessible by experiments but it contains essential physical information concerning the behavior of strongly interacting systems. The most well-known example of that is the Banks-Casher relation implying that a non-vanishing Dirac spectral density at zero indicates the spontaneous breaking of chiral symmetry [1]. Another prominent example is that in the intermediate volume, so called “epsilon regime,” the lowest part of the Dirac spectrum is described by random matrix theory (RMT), which makes it possible to extract the low-energy constants of chiral perturbation theory from the eigenvalues of the Dirac operator (see e.g., Ref. [2] and references therein). More recently the Dirac spectrum has also been used to determine the mass anomalous dimension of QCD-like theories with many fermions [3–6].

Since at low temperature the low-lying Dirac spectrum has been so extensively studied it is surprising how little is known about it in the high-temperature regime. The only solid piece of information above the finite temperature crossover is that since chiral symmetry is restored there the spectral density of the Dirac operator should vanish at zero. In principle, random matrix theory also has predictions for the spectral statistics at such a “soft edge.” However, unlike at zero temperature, at high temperature *a priori* there is no reason to believe that the QCD Dirac spectrum is described by this edge RMT statistics. Indeed, attempts to verify this numerically did not produce fully convincing results [7,8].

It turns out that random matrix statistics is only one of two possible extremes concerning the eigenvalue statistics.

It corresponds to the case of completely delocalized eigenvectors occurring only if typical (gauge field) fluctuations can easily mix eigenmodes nearby in the spectrum. The other extreme possibility is localized eigenmodes that cannot be mixed by typical fluctuations. In that case the spectrum consists of independent eigenvalues obeying Poisson statistics. Many examples of both types of behavior in large linear systems are known both in the mathematics and in the physics literature. In fact the Bohigas-Giannoni-Schmit conjecture asserts that quantum systems whose classical counterparts are chaotic exhibit random matrix-type spectra whereas integrable systems after quantization have Poisson-type spectra [9]. An example where the same physical system, depending on the circumstances, can exhibit both types of behaviors is Anderson localization [10]. In that case the transition of single electron states from delocalized ones described by RMT statistics to localized states with Poisson statistics is driven by impurities in the crystal lattice.

Already a long time ago the idea was put forward that such a transition might also occur in QCD at finite temperature [11]. Later on numerical studies concluded that it is not the case and the Dirac spectrum is described by RMT even above the finite temperature deconfining and chiral transition [12]. This conclusion, however, was based on the study of full Dirac spectra. It is known that in the case of the Anderson transition for weak disorder only the states along the band edge become localized and states deep inside the band can still remain delocalized. Therefore a statistical analysis of full spectra might not reveal a localization transition occurring only along the band edge.

With this additional insight the idea of a localization-delocalization transition in QCD at T_c was revived sometime later [13]. Both instanton liquid calculations [14] and lattice QCD simulations were [15] done to provide evidence that such a transition occurs at T_c . However, these

*Present address: Institute for Nuclear Research of the Hungarian Academy of Sciences, Bem tér 18/c, H-4026 Debrecen, Hungary.

calculations were performed around the critical temperature and therefore it was not possible to see clear Poisson statistics in the spectrum. For that lattice simulations were needed well above T_c where localized modes are fully developed. Indeed, further support for localization in QCD was obtained by a detailed demonstration that the lowest two eigenvalues of the overlap Dirac operator in quenched $SU(2)$ gauge theory obey Poisson statistics [16]. Finally in the same system a clear transition was observed in the spectrum of the staggered Dirac operator from localized Poisson modes to delocalized RMT modes [17]. The picture emerging from these studies is that above the finite temperature transition the lowest part of the Dirac spectrum consists of localized modes obeying Poisson statistics. Higher up in the spectrum there is a crossover to delocalized modes described by random matrix statistics. In the meantime, independently, other groups also observed the tendency of low modes to become localized above T_c [18], although the connection to an Anderson-type transition was not made by them. A useful account of the spatial structure of low Dirac modes and their localization properties can also be found in Ref. [19].

So far all the direct evidence for the transition came from quenched $SU(2)$ simulations. In the present paper we study the question whether full QCD with physical light dynamical quarks also exhibits delocalized Dirac modes above T_c . The question is nontrivial since light dynamical quarks suppress the lowest quark modes through the quark determinant in the action. Nevertheless we find that localization also occurs in full QCD with quarks of physical masses. We demonstrate this by presenting the results of lattice QCD simulations with $N_f = 2 + 1$ flavors of dynamical staggered quarks. We also study how the location of the transition within the spectrum depends on the physical temperature.

The paper is organized as follows. At first in Sec. II we summarize the technical details of our QCD lattice simulations. In Sec. III we describe the analogy between the QCD delocalization-localization transition and the Anderson transition. Here we analyze in detail the unfolded level spacing distribution that can be used to distinguish between localized and delocalized modes. We show that in larger spatial volumes the transition becomes sharper and most likely in the thermodynamic limit it becomes a genuine phase transition. Also in this section we show how to compute the mobility edge separating localized and delocalized states in the spectrum and analyze localization in terms of the participation ratio of eigenmodes. In Sec. IV we study how the transition scales in the continuum limit. In particular, we show that the localization length of localized states is always smaller than the inverse temperature. We also demonstrate that the properly renormalized mobility edge scales in the continuum limit and investigate its temperature dependence in the temperature range $1.7T_c < T < 5T_c$. Finally, in Sec. V we summarize our results and indicate further questions.

II. SIMULATION DETAILS

At first we summarize the details of our lattice simulations. We use the Symanzik improved gauge and the two level stout smeared staggered fermion action of Ref. [20] with $N_f = 2 + 1$ flavors. We take the simulation parameters from the work of the Budapest-Wuppertal Collaboration who determined the lattice spacing from the kaon decay constant f_K and set the bare quark masses by requiring the pion and kaon masses to be equal to their physical value [21]. The bare parameters we used and the corresponding lattice spacings are summarized in Table I.

To explore the dependence of the localized-delocalized mode transition on the temperature and the lattice spacing we performed the simulations at three different lattice spacings $a = 0.06, 0.082$ and 0.125 fm and three different temporal lattice extensions $N_t = 4, 6, 8$. The physical temperature of the system is set by its temporal extension as

$$T = \frac{1}{N_t a}. \quad (1)$$

In this way the lattice parameters we used correspond to the physical temperature range of $1.7T_c < T < 5T_c$.

To understand the nature of the transition it is crucial to consider the spatial volume dependence of spectral and wave function statistics. For this reason we also repeated some simulations on different spatial volumes. The spatial linear size of the boxes we used were all in the range $2 \text{ fm} \leq L \leq 6 \text{ fm}$. The details of the parameters of our ensembles are summarized in Table II.

Since low Dirac modes can potentially be slow modes of the system we also checked for autocorrelations. In a long run performed on the finest lattice we found that the autocorrelation time for the smallest Dirac modes is definitely smaller than ten trajectories. To be on the safe side on the finest lattice the configurations that we used for spectrum calculations were always separated by 30 trajectories. Even on the coarsest lattice, configurations were separated by ten trajectories.

III. ANDERSON TRANSITION IN THE DIRAC SPECTRUM

Previously it was seen that in the high temperature deconfining phase of $SU(2)$ Yang-Mills theory there is a transition in the staggered Dirac spectrum from localized

TABLE I. The bare parameters we used in the lattice simulations: the inverse gauge coupling (β), the light quark mass (m_{ud}), the strange quark mass (m_s) and the corresponding lattice spacing (a).

β	m_{ud}	m_s	a (fm)
3.75	0.001786	0.05030	0.125
3.938	0.001172	0.03300	0.082
4.08477	0.000836	0.02354	0.062

TABLE II. The parameters of the simulations: the temperature, the lattice spacing, the spatial and temporal box size, the inverse gauge coupling, the number of configurations and the number of Dirac eigenvalues computed on each configuration.

	T (MeV)	a (fm)	N_s	N_t	Nconf	Nevs
A1	263	0.125	24	6	430	512
A2			36		420	256
B	300	0.082	32	8	434	256
C1	394	0.125	16	4	1622	512
C2			24		1600	512
C3			32		900	512
C4			48		604	128
D1	401	0.082	24	6	440	512
D2			36		440	256
E	397	0.062	32	8	593	256
F	530			6	420	512
G	601	0.082	24	4	396	512
H	794	0.062	32	4	417	512

low modes to delocalized modes higher up in the spectrum [17]. The question we ask here is whether such a transition also occurs in real QCD with light dynamical quarks. This is a nontrivial question since light quarks suppress low Dirac modes through the fermion determinant in the functional integral and in the quenched case it is exactly the lowest Dirac modes that are localized.

The hallmark of a transition from localized to delocalized modes in terms of spectral statistics is a change from Poisson statistics to random matrix statistics in the spectrum. Intuitively speaking, localized modes are such because they cannot mix with other modes; typical gauge field fluctuations do not mix them. Localized modes close in the spectrum are peaked at spatially distant locations and they are sensitive only to gauge field fluctuations there. As a result the corresponding eigenvalues are statistically independent and the level spacings obey Poisson statistics. Delocalized modes, in contrast, are mixed by typical gauge field fluctuations. Gauge field fluctuations change several delocalized modes together which introduces delicate correlations in the spectrum and as a result the eigenvalue statistics is described by RMT.

The simplest way to detect a transition in the spectrum from Poisson to RMT statistics is to consider the so-called unfolded level spacing distribution. Unfolding is essentially a local rescaling of the eigenvalues to have unit spectral density throughout the spectrum. We did the unfolding by ordering all eigenvalues in the given ensemble and replacing them with their rank order normalized by the total number of configurations. On a few ensembles we also checked unfolding by using local spline approximations to the spectral density but there was no discrepancy between the two methods of unfolding.

Since the unfolded level spacing distribution (ULSD) is known analytically for both the Poisson and the RMT

statistics it can be easily used to distinguish between the two cases. For Poisson statistics the ULSD is a simple exponential,

$$P_{\text{Poisson}}(s) = \exp(-s).$$

In the RMT case the unfolded level spacing distribution depends on the universality class which in the case of staggered fermions in the fundamental representation of the $SU(3)$ gauge group is the chiral Unitary Ensemble (chUE) [2]. The corresponding ULSD is very precisely approximated by the chiral unitary Wigner surmise,

$$P_{\text{chUE}}(s) = \frac{32}{\pi^2} s^2 \cdot \exp\left(-\frac{4}{\pi} s^2\right). \quad (2)$$

To demonstrate the transition in the spectrum in Fig. 1 we plot the ULSD in different regions of the spectrum of ensemble C3: $0.15 \leq \lambda a \leq 0.19$ (a), $0.29 \leq \lambda a \leq 0.32$ (b), $0.34 \leq \lambda a \leq 0.35$ (c) and $0.375 \leq \lambda a \leq 0.385$ (d). We also indicate in the same figure the distributions corresponding to the Poisson (localized) and the RMT (delocalized) case. The transition from localized modes at the edge of the spectrum to delocalized modes in the bulk can be clearly seen. This shows that light dynamical fermions do not change the picture observed in the quenched case earlier and the transition also occurs in QCD with quarks of physical masses.

To give a qualitative picture of how the spectral density goes, in Fig. 2 we plot the integrated spectral density on ensemble C3. For comparison we also included in the same figure data for the ensemble C2 with the same parameters,

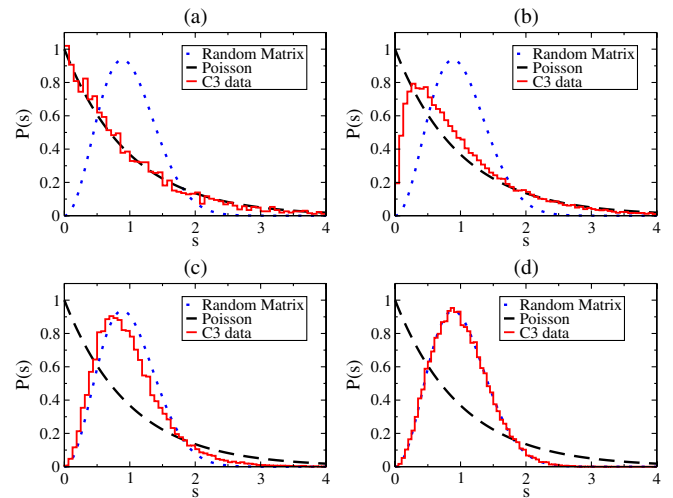


FIG. 1 (color online). The unfolded level spacing distribution in different regions of the spectrum of ensemble C3. The figures correspond to the spectral regions $0.15 \leq \lambda a \leq 0.19$ (a), $0.29 \leq \lambda a \leq 0.32$ (b), $0.34 \leq \lambda a \leq 0.35$ (c) and $0.375 \leq \lambda a \leq 0.385$ (d). The dashed line indicates the exponential distribution corresponding to the localized (Poisson) case and the dotted line indicates the chiral unitary Wigner surmise expected in the delocalized (RMT) case.

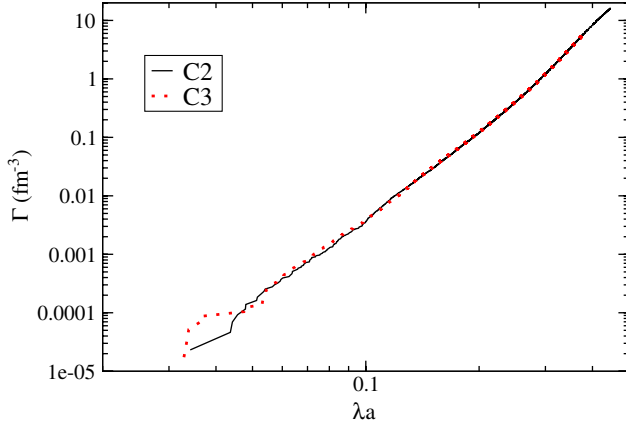


FIG. 2 (color online). The integrated spectral density in units of number of eigenvalues per cubic Fermi. We compare data from ensembles C2 and C3 which are almost identical except that the spatial linear sizes are 3 fm and 4 fm, respectively.

but smaller spatial volume. The data show good scaling with the three-volume that we also observed on other ensembles. Comparing this figure with the spectral windows depicted in Fig. 1 one can observe that in the Poisson regime the integrated spectral density is much smaller than unity. In the transition region it becomes comparable to unity and finally in the Wigner-Dyson (RMT) regime it becomes much bigger than that.

A. Analogy with the Anderson transition

The transition in the spectrum from localized to delocalized modes is reminiscent of the Anderson metal-insulator transition occurring in conducting crystalline solids when impurities are introduced [10]. In that case in the presence of impurities single electron Bloch states along the band edge turn into localized states. In three dimensions if the impurity concentration is not too high, states at the band center can still remain delocalized. The boundary between localized and delocalized states is known as the mobility edge. Increasing the density of impurities pushes the mobility edge further towards the center of the band until all the states in the band become localized. When the mobility edge passes the Fermi energy and the Fermi energy gets into the delocalized part of the spectrum the system has a vanishing zero-temperature conductivity. The states that can be excited are all nonconducting localized states.

It has been conjectured that the finite temperature QCD transition might be similar to the Anderson transition [13]. Further indications to support this picture were obtained from instanton liquid [14] and lattice QCD simulations [15].

We now sketch the analogy between the spectrum of the one electron Hamiltonian in disordered media and that of the QCD Dirac operator. Due to the symmetries of the QCD Dirac operator its spectrum is symmetric with respect to the real axis. In the continuum and also in the case of the staggered lattice Dirac operator, the one we use here, the

spectrum is purely imaginary. That is if the quark mass is zero, otherwise the quark mass provides a trivial real part to all the eigenvalues. In the chiral limit (zero quark mass) the spectral density at zero is proportional to the chiral condensate, the order parameter of spontaneous chiral symmetry breaking [1]. At high enough temperature chiral symmetry is restored and the spectral density at zero vanishes. In that case the spectrum has a so-called “soft edge” and there might even be a gap around zero in the spectrum [7,8]. This “edge” of the spectrum at the low end is analogous to the band edge in condensed matter systems.

In the condensed matter literature numerical studies of the Anderson transition usually concentrate on the band center and locate the critical disorder when states at the center become localized. As we will see, in the case of QCD the location of the mobility edge is controlled by the temperature and there is no analog of the band center since the spectral density continues to be nonzero all the way up to the cutoff scale. Therefore, unlike in most of the condensed matter literature, here we do not attempt to determine the critical disorder where all delocalized states disappear but rather study how the mobility edge changes with the temperature. This approach is not completely unknown in the condensed matter literature either [22].

B. Second moment of the unfolded level spacing distribution

As can be seen in Fig. 1 the unfolded level spacing distribution changes in the spectrum from the exponential to the Wigner surmise in a continuous fashion. There does not appear to be a sharp mobility edge λ_c separating localized and delocalized states. Even in the case of Anderson transitions, however, a sharp transition is expected only in the thermodynamic limit when the spatial size of the system N_s goes to infinity. This is completely analogous to second order phase transitions where a truly divergent correlation length and a sharp phase transition can only be observed in infinite systems. In principle any physical quantity that changes in a well-defined way from the localized to the delocalized regime can be used to define a transition point in the spectrum. If there is a sharp transition in the thermodynamic limit then nonanalytic behavior should appear in all these quantities at a given point λ_c in the spectrum. In what follows we will look for a quantity that can be used to define the transition point.

Since the first moment of the unfolded level spacing distribution is unity by construction, the simplest quantity to consider is its second moment or variance. In the localized case the level spacings are exponentially distributed and the variance is

$$\sigma_s^2 = \langle s^2 \rangle - \langle s \rangle^2 = 1, \quad (3)$$

while in the delocalized regime the second moment of the distribution of Eq. (2) can be analytically determined to be $\sigma_s^2 = \frac{3\pi}{8} - 1$. In Fig. 3 we plot how the variance changes in

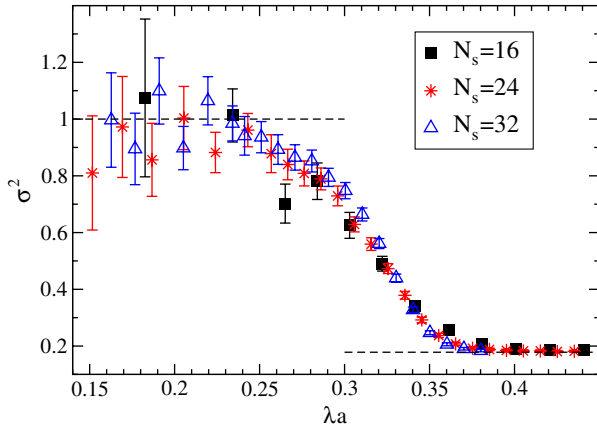


FIG. 3 (color online). Variance of the unfolded level spacing distribution across the transition in the spectrum for ensembles C1, C2 and C3 that differ only in their spatial volume. The dashed horizontal lines at 1 and 0.178 indicate the expected limits in the localized (Poisson) and delocalized (RMT) regime.

the spectrum throughout the transition region. We computed the variance of the unfolded level spacing distribution in small spectral windows. We checked that the variances were independent of the chosen width of the spectral windows; regardless of the window size the points lay on the same smooth curve. For each ensemble we chose a window size to obtain reasonable spectral resolution with acceptable statistical errors. The three data sets correspond to ensembles C1–C3 with three different spatial volumes but otherwise identical parameters. It is apparent that with increasing volume the transition becomes sharper. To define a finite volume pseudocritical point in the spectrum we locate the inflection point of the curve $\sigma^2(\lambda)$. To this end we use the three-parameter fitting ansatz

$$\sigma^2(\lambda) = A\{1 - \tanh(B(\lambda - C))\} + \frac{3\pi}{8} - 1. \quad (4)$$

This form ensures the correct limit for large λ and yields good fits starting already from $\lambda a = 0.2, 0.25$ i.e., already from below the transition point. Using this ansatz the inflection point can be easily seen to be at $\lambda_c a = C$ and the slope of the curve there is AB . These two parameters are largely independent of the starting point of the fit as long as it starts at smaller values of λ than where the inflection point occurs. The location of the inflection point turns out to be also independent of the volume yielding pseudocritical points $C = \lambda_c a = 0.321(4), 0.322(1), 0.324(2)$ for the spatial sizes $N_s = 16, 24, 32$. The slope at the inflection point is $AB = 7.6(5), 10.96(36), 13.8(5)$ for the three different spatial sizes and it scales roughly proportionally to the linear spatial size of the box. This indicates that there might be a genuine sharp transition in the thermodynamic limit. The sharpening of the transition with the volume can be better seen in Fig. 4 where we plot again the variance of the unfolded level spacing distribution but

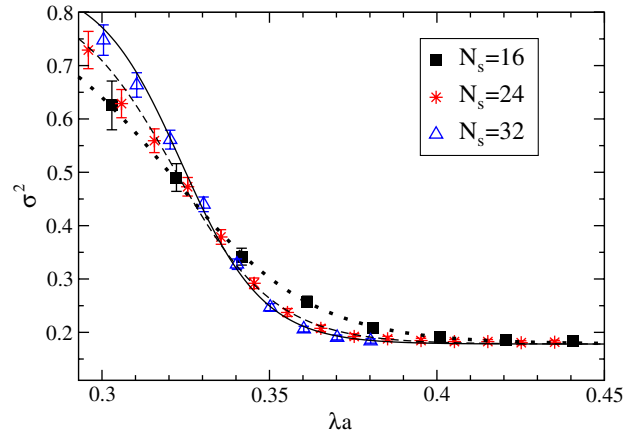


FIG. 4 (color online). The same as Fig. 1 but zooming in on the transition region. The dotted, dashed and the continuous curve indicate the fits of the form Eq. (4) to the $N_s = 16, 24$ and 32 data, respectively.

zoom in on the transition region and also show the fitted curves with the above described parameters.

C. Eigenvector statistics

Besides the spectrum the spatial profile of the corresponding eigenvectors also contains important information concerning their localization properties. A quantity that is widely used in this context is the inverse participation ratio (IPR) defined as [23]

$$P_\psi = \sum_x |\psi(x)|^4, \quad (5)$$

where ψ is an eigenvector normalized as

$$\sum_x |\psi(x)|^2 = 1. \quad (6)$$

The qualitative physical meaning of the IPR can be easily seen by noting that an eigenmode that spreads uniformly in a four-volume v and is zero everywhere else has $\text{IPR} = 1/v$. The IPR^{-1} thus measures the volume occupied by an eigenmode. Alternatively one can use the participation ratio, $\text{PR} = \text{IPR}^{-1} \cdot V^{-1}$, where V is the total volume of the system. This measures the fraction of the total volume occupied by the eigenmode.

The behavior of the IPR and the PR in the thermodynamic limit can be used to distinguish between localized and delocalized modes. By definition a part of the spectrum consists of localized modes if their average IPR remains finite as the volume goes to infinity. This also implies that their average PR vanishes in the thermodynamic limit. In contrast delocalized modes have vanishing IPR which usually implies nonvanishing PR.

In Fig. 5 we plot how the average participation ratio of eigenmodes changes throughout the spectrum on ensembles C1–C4. The four data sets correspond to different spatial sizes but otherwise identical parameters. It is clearly seen that the average PR for the low eigenmodes decreases as the

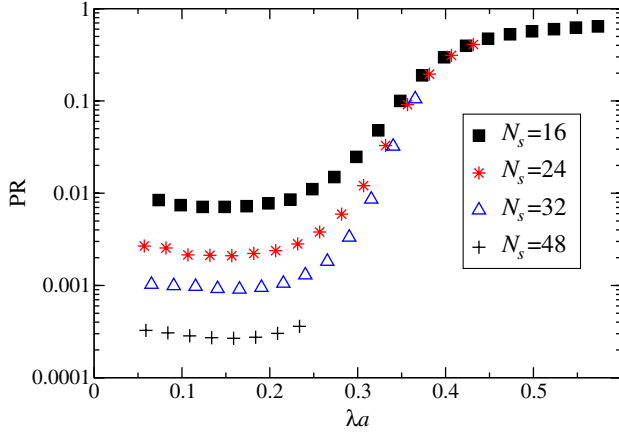


FIG. 5 (color online). Average PR of the eigenvectors for lattices with the same temperature and lattice spacing but with four different aspect ratios $N_t = 4$.

volume is increased; the average PR here tends to zero in the thermodynamic limit. This suggests that these eigenmodes are localized. They fill a vanishing fraction of the total box volume in the thermodynamic limit. Higher up in the spectrum the average PR becomes a volume independent constant of order unity, which means that these eigenmodes are delocalized. They fill a nonzero fraction of the total box volume in the thermodynamic limit.

IV. CONTINUUM LIMIT AND RENORMALIZATION

We saw that on all the ensembles that we considered there is a critical point (“mobility edge”) λ_c in the Dirac spectrum that separates localized and delocalized eigenmodes. If the lowest part of the spectrum becomes localized that can have a dramatic effect on long distance correlators of quark operators and the masses associated with them. This happens because in the spectral decomposition of the quark propagator $(D + m)^{-1}$ each eigenmode is weighted by the inverse of the corresponding eigenvalue. Therefore the lowest eigenmodes receive the largest weight. On the other hand, eigenmodes localized to a distance scale l have negligible contribution to correlators at distance scales much larger than l .

To assess the physical implications of localization in QCD we are thus lead to study two questions:

- (1) What is the distance scale l on which the lowest eigenmodes are localized?
- (2) How far up in the spectrum (λ_c) are the modes localized?

Both of these questions have to be considered in the continuum limit as the lattice spacing $a \rightarrow 0$.

A. Localization length

To get a rough estimate of the localization scale we can consider the IPR defined by Eq. (5). Since the IPR scales

like the inverse four-volume of the region where the given mode is spread out a good measure of the localization scale is provided by the quantity

$$l = a \cdot \langle \text{IPR}^{-\frac{1}{4}} \rangle, \quad (7)$$

where the average is understood over all the eigenmodes in a given region of the spectrum. In principle l varies through the spectrum but it does not change too much within the region of localized modes. To illustrate that, in Fig. 6 we show in two representative cases how l changes through the spectrum. As can be seen in the figure for the lowest part of the spectrum the localization length is almost constant and is independent of the spatial volume. In this region there might be a small dip in l . The dip is generally more pronounced at lower temperatures and/or on finer lattices but on our ensembles the total variation of l in the localized regime never exceeds 20%. At some point in the spectrum l starts to increase sharply and becomes strongly volume dependent. This is the beginning of the transition to delocalized states.

In what follows we define the localization length of localized modes with the following simple procedure. The localized eigenmodes all have l 's between the bottom of the dip and the l of the very lowest eigenmodes. This interval for ensembles D1 and D2 is indicated by the two dashed horizontal lines in Fig. 6. The central value we quote for l is always the center of this band and the uncertainty is half the width of the band. Compared to that, statistical errors are always negligible.

Having a well-defined measure of the localization length for localized modes we can now look at how it depends on the lattice spacing. Since, as we will see, l also depends on the temperature, we choose to compare ensembles C, D and E which are almost exactly at the same physical temperature of about 400 MeV. Since l does not depend on the spatial volume we omit the numbers from the

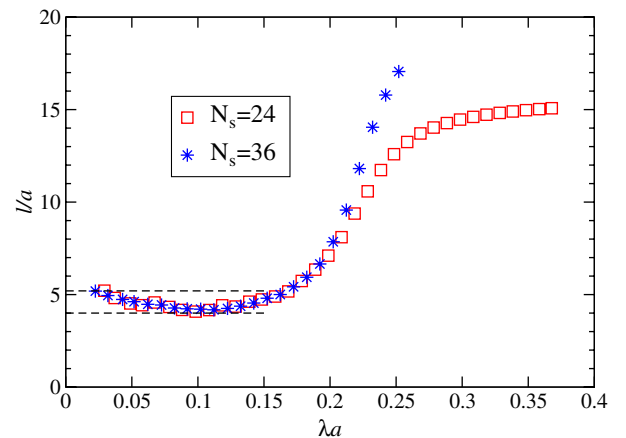


FIG. 6 (color online). The localization length [Eq. (7)] of eigenmodes along the spectrum for ensembles D1 and D2 differing only in their spatial volumes. Both l and the location in the spectrum λ are given in lattice units. Statistical errors are not shown as they are smaller than the size of the symbols.

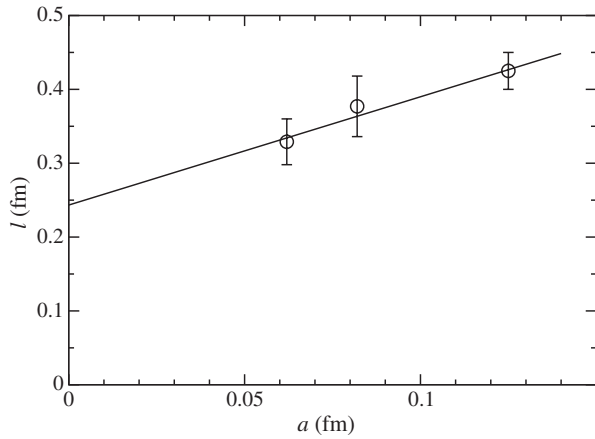


FIG. 7. The localization length of the localized modes as a function of the lattice spacing. The three points correspond to the same physical temperature of about 400 MeV (ensembles C, D and E).

ensemble labels here. In Fig. 7 we plot the localization length as a function of the lattice spacing for these three ensembles.

To guide the eye we also included a linear fit to the data. Even if the quality of our data does not allow a proper continuum extrapolation it can be safely concluded that the localization length measured in physical units does not increase in the continuum limit and it is not larger than a few tenths of a Fermi at this temperature.

It is also instructive to see how the localization length compares to the most important length scale in the problem, the inverse temperature or in other words the temporal size of the box. In Fig. 8 we plot the localization length in units of the inverse temperature for all the ensembles. Different symbols represent data sets corresponding to different values of the lattice spacing. There is a slight trend of the finer lattices producing more localized low

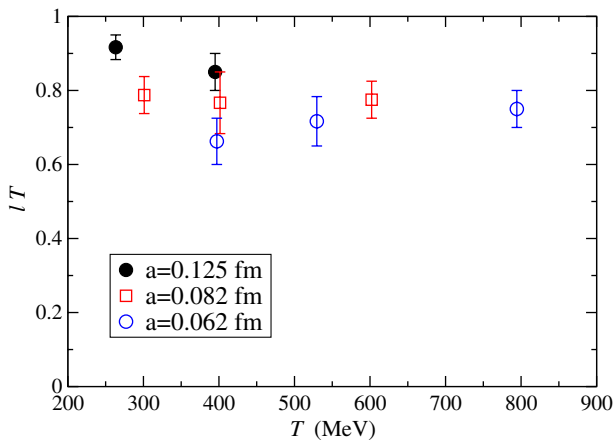


FIG. 8 (color online). The localization length in units of the inverse temperature as a function of the physical temperature. The different symbols represent data obtained at different values of the lattice spacing.

modes as can be seen also in Fig. 7. The important point is that the lowest modes always appear to be localized on or below the scale of the inverse temperature in the whole range of temperatures studied here.

B. Renormalization and temperature dependence of λ_c

We have seen that the lowest eigenmodes spread out only to a distance scale below the inverse temperature. Therefore these modes cannot contribute to quark propagation on length scales larger than that. As far as hadronic correlators are considered, above that distance scale the system behaves as if it had a gap of order λ_c . The influence of this effective gap on the physics depends on how λ_c , the critical point in the spectrum, scales in the continuum limit.

In Sec. III B we showed how to determine the critical point using the second moment of the unfolded level spacing distribution. This procedure yields the critical point $\lambda_c a$ in dimensionless lattice units for each temperature and lattice spacing. In what follows we give a proposal for defining the continuum limit of this quantity. Since the critical point is effectively a gap for quark modes capable of propagating to long distances it plays a role similar to the quark mass that also introduces a gap. For this reason we expect λ_c to be renormalized in exactly the same way as the quark mass and the ratio of $\lambda_c a$ to the bare light quark mass $m_{ud} a$ should have a proper continuum limit. Moreover this quantity measures the relative size of the effective gap for delocalized modes and the gap for all modes provided by the quark mass.

Another, perhaps more formal, argument showing that λ_c/m_{ud} has a well-defined continuum limit is as follows. On the one hand, the pseudoscalar meson correlator $\langle P(x)P(0) \rangle$ is proportional to the matrix elements of the square of the Dirac propagator, $[(D^\dagger + m)(D + m)]^{-1}$. On the other hand, for asymptotically large temporal separations t

$$\frac{1}{V_s} \sum_{\vec{x}} \langle P(t, \vec{x})P(0) \rangle = C_{PP} e^{-m_\pi t}, \quad (8)$$

where V_s is the spatial volume and C_{PP} is related to the pion decay constant f_π as [24]

$$C_{PP} m_{ud}^2 = \frac{f_\pi^2}{V_s} m_\pi^3. \quad (9)$$

The right-hand side of this equation is a well-defined physical quantity and thus so is the left-hand side. Since C_{PP} is proportional to the inverse quark propagator squared, it is also proportional to the inverse of the Dirac eigenvalues squared. Thus

$$m_{ud}^2 \lambda_c^{-2} \propto C_{PP} m_{ud}^2 \quad (10)$$

also has a well-defined continuum limit. For a more general discussion of similar issues with Wilson fermions see also Refs. [25,26].

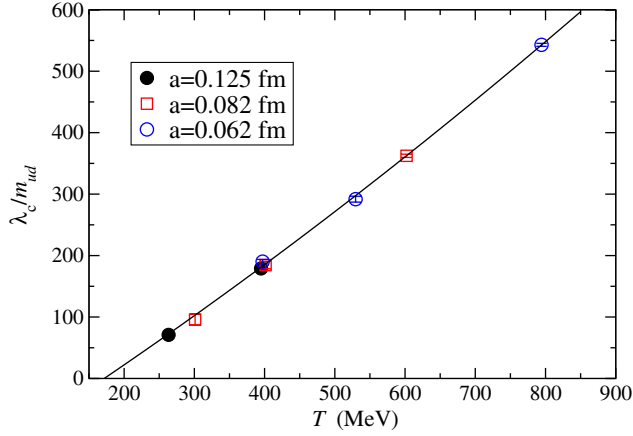


FIG. 9 (color online). The temperature dependence of the renormalized critical point $\frac{\lambda_c}{m_{ud}}$. The continuous line is a second order polynomial fit to all the data. The different symbols correspond to data obtained using lattices of different coarseness.

Data sets C, D and E where we have data at the same temperature for all three lattice spacings indicate that the lattice spacing dependence in the quantity $\frac{\lambda_c}{m_{ud}}$ is comparable to its uncertainty at a given lattice spacing. Therefore in Fig. 9 we plot the temperature dependence of this quantity for all lattice spacings in the same figure. The different types of symbols corresponding to data obtained from lattices of different coarseness all lie on a smooth curve confirming that scaling violations in this quantity are small. A three-parameter fit to the data of the form

$$\frac{\lambda_c}{m_{ud}} = a \cdot \frac{T - T_c}{T_c} + b \cdot \left(\frac{T - T_c}{T_c} \right)^2 \quad (11)$$

yields $a = 133(14)$, $T_c = 171(9)$ MeV, $b = 4(1)$ with an acceptable chi squared of $\chi^2 = 1.3$. Although putting b to zero the two-parameter linear fit results in a two times larger chi squared [with $T_c = 191(6)$ MeV], in the whole range of the data the two curves are barely distinguishable by the naked eye. This means that to a very good approximation the mobility edge depends linearly on the temperature. For clarity, in the figure we show only the three-parameter fit. It is also obvious from the fit function that $\frac{\lambda_c}{m_{ud}}$ vanishes at $T_c = 171$ MeV which we identify with the pseudocritical temperature below which localized states are not expected at all. This value is consistent with the known location of the finite temperature crossover in QCD [27,28]. This provides a further consistency check of our results.

Another physically interesting quantity is the number density of localized modes. This quantity is also practically important if one aims at detecting localization from spectral statistics. In order to be able to observe Poisson statistics in the level spacing distribution the volume of the system has to be large enough to accommodate several localized eigenmodes per configuration. To see what that

means practically in Fig. 10 we plotted the average density of eigenmodes below λ_c as a function of the temperature. Again we collect data obtained at different values of the lattice spacing in the same figure. Apparently the number density of localized modes decreases sharply as the transition temperature is approached from above. In practical terms that means that in order to have for instance about 20 localized modes per configuration the aspect ratio of the boxes has to be kept between 4–6 in the temperature range considered here.

Finally we would like to point out a potential technical difficulty in studying the level spacing distribution. It is caused by the pairing of staggered Dirac eigenvalues affecting the lowest part of the spectrum when the spatial volume is small. It comes about because in the continuum limit staggered fermions describe four fermion flavors and the spectrum is expected to become fourfold degenerate. Therefore approaching the continuum limit this degeneracy starts to be formed and peculiar correlations will appear among members of the would-be continuum quartets.

It turns out that already at the lattice spacings we used here the stout smearing of gauge fields coupled to the fermions brings the spectrum close enough to the continuum behavior that such extra correlations for the lowest eigenvalues can be detected. This is first manifested in pairwise attraction between consecutive eigenvalues which distorts the Poisson statistics [29,30]. To illustrate this, in Fig. 11 we plot the average of the lowest eight eigenvalues for three ensembles with the same physical volume and temperature differing only in the lattice spacing. The formation of doublets on the finer grids is obvious in the figure but the quartet structure does not appear even on the finest grid. It is also obvious from the figure that as we go up in the spectrum and the spectral density increases rapidly

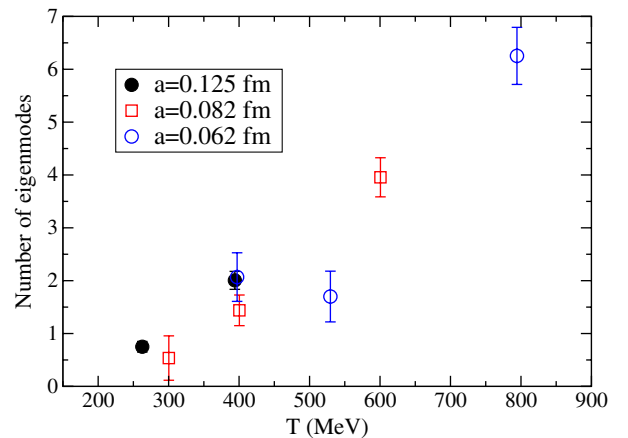


FIG. 10 (color online). The number of localized (below λ_c) eigenmodes per cubic Fermi as a function of the temperature. Different symbols refer to simulations at different values of the lattice spacing.

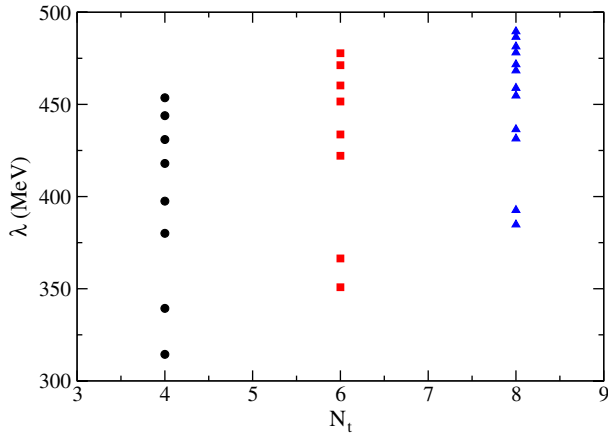


FIG. 11 (color online). The average of the lowest eight eigenvalues for ensembles C1 ($N_t = 4$), D1 ($N_t = 6$) and E ($N_t = 8$). The error bars are comparable to the size of the symbols and for clarity they have been omitted.

(cf. Fig. 2) the distance between doublets decreases much more rapidly than the splitting within the doublets. As a result, above the first few doublets even the doublet structure is completely washed out by the increasing spectral density. Since the spectral density is proportional to the volume, this happens even faster in larger volumes. As a result, if the lowest spectral window in which spectral statistics are computed is wide enough and the volume is large enough, doublet formation does not distort the Poisson statistics significantly.

As a matter of principle, we have to admit that since the quartet structure expected in the continuum has not yet formed in our simulations, spectral and eigenvector statistics might be different in the continuum. It is even not clear to us how exactly this quartet structure should appear and scale especially in the thermodynamic limit where the level spacing should go to zero. On the other hand, we do not expect this to qualitatively change the localization and statistical properties of the eigenvectors. In previous studies of the $SU(2)$ quenched theory we used both staggered and overlap fermions and found qualitatively similar localized eigenmodes and similar spectral statistics [16,17]. Moreover, on the same gauge backgrounds the location of staggered and overlap eigenmodes were strongly correlated [31]. Thus we expect that staggered and overlap fermions see the same universal physical features and it is likely that localization persists in the continuum limit. However, to establish that absolutely certainly one would need to repeat our present study with dynamical overlap fermions.

Finally, we also would like to add a remark about the possible effects of topological charge on the spectral statistics. In principle, even staggered fermions are expected to have small near-zero modes in the presence of a nonzero topological charge. However, our experience in the quenched $SU(2)$ case shows that at the temperatures we

study here, fluctuations of the total topological charge are rather small [16]. Moreover, the number of topological near-zero modes scales only with the square root of the volume whereas the number of nontopological modes goes with the volume. Therefore in our large volumes we do not expect topological near-zero modes to have a significant distorting effect on spectral statistics.

V. CONCLUSIONS

In the present paper we argued that in QCD above the finite temperature crossover the lowest eigenmodes of the quark Dirac operator are localized. The spatial localization length is set by the inverse temperature (see Fig. 8) with eigenmodes becoming more “squeezed” at higher temperature. At the same time when the temperature increases the mobility edge, separating localized and delocalized modes, is also pushed higher up in the spectrum.

This high temperature behavior of the low Dirac modes has to be contrasted with the situation at low temperature below the crossover. In that case chiral symmetry is spontaneously broken and a finite density of eigenmodes extends down all the way to zero. As a result, the statistics of the lowest Dirac modes is described by random matrix theory. QCD is thus a remarkably rich theory. The low end of the Dirac spectrum can exhibit both possible extremes of spectral statistics: maximally mixed modes with RMT statistics below the transition and completely independent eigenmodes with Poisson spectral statistics at high temperature.

The localization of the lowest Dirac modes can dramatically suppress hadronic correlators at high temperatures. In the eigenmode expansion of the quark propagator the lowest part of the spectrum receives the largest relative weight. If, as we saw, these modes are localized they cannot propagate quarks to long distances resulting in a suppression of long-distance correlators. As can be seen in Fig. 9 the mobility edge below which all states are localized moves steeply up with increasing temperature. Already at $2T_c$ it is two orders of magnitude larger than the bare light quark mass. This mechanism might help to explain the steep rise of screening masses above T_c seen in lattice simulations [32].

An interesting question is how exactly the spectral and wave function statistics change through the mobility edge and whether there is any universality in how these quantities interpolate between the localized and delocalized regime. In particular we would like to check whether the scale invariance of the inverse participation ratio distribution observed in Anderson transitions [33] also occurs in the QCD transition. We hope to return to this question in a future publication. As far as the Poisson to RMT transition in the spectral statistics is concerned there does not seem to be a universal understanding of how it happens in general but there are several proposals that might provide further insight [31,34–36].

It would also be interesting to know what physical mechanism drives the transition. Is it possible to identify some physical objects in the gauge field background that are responsible for the appearance of localized modes? In a previous paper some evidence was found that there is a correlation between localized modes and local fluctuations of the Polyakov loop [31]. On the other hand it was also argued there that uncorrelated instantons cannot play a significant role in this mechanism as their density is too low for that. It is, however, still possible that instanton molecules or “bions” have to do with localization [37]. A better understanding of the physical mechanism behind

localization in QCD could possibly shed some more light on the finite temperature chiral and deconfining transition.

ACKNOWLEDGMENTS

T.G.K. is supported by the Hungarian Academy of Sciences under “Lendület” Grant No. LP2011-011. Both authors acknowledge partial support by the EU (FP7/2007-2013)/ERC Grant No. 208740. We thank the Budapest-Wuppertal group for allowing us to use their computer code for generating the lattice configurations. Finally we also thank S. D. Katz and D. Nógrádi for discussions.

-
- [1] T. Banks and A. Casher, *Nucl. Phys.* **B169**, 103 (1980).
- [2] J. J. M. Verbaarschot and T. Wettig, *Annu. Rev. Nucl. Part. Sci.* **50**, 343 (2000).
- [3] T. DeGrand, [arXiv:0906.4543](https://arxiv.org/abs/0906.4543); *Phys. Rev. D* **80**, 114507 (2009).
- [4] L. Del Debbio and R. Zwicky, *Phys. Rev. D* **82**, 014502 (2010).
- [5] A. Patella, *Phys. Rev. D* **86**, 025006 (2012).
- [6] A. Cheng, A. Hasenfratz, and D. Schaich, *Phys. Rev. D* **85**, 094509 (2012); A. Hasenfratz, A. Cheng, G. Petropoulos, and D. Schaich, *Proc. Sci., LATTICE2012* (2012) 034 [[arXiv:1207.7162](https://arxiv.org/abs/1207.7162)].
- [7] F. Farchioni, P. de Forcrand, I. Hip, C. B. Lang, and K. Splittorff, *Phys. Rev. D* **62**, 014503 (2000).
- [8] P. H. Damgaard, U. M. Heller, R. Niclasen, and K. Rummukainen, *Nucl. Phys.* **B583**, 347 (2000).
- [9] O. Bohigas, M. J. Giannoni, and C. Schmit, *Phys. Rev. Lett.* **52**, 1 (1984).
- [10] P. W. Anderson, *Phys. Rev.* **109**, 1492 (1958).
- [11] A. M. Halasz and J. J. M. Verbaarschot, *Phys. Rev. Lett.* **74**, 3920 (1995).
- [12] R. Pullirsch, K. Rabitsch, T. Wettig, and H. Markum, *Phys. Lett. B* **427**, 119 (1998).
- [13] A. M. Garcia-Garcia and K. Takahashi, *Nucl. Phys.* **B700**, 361 (2004).
- [14] A. M. Garcia-Garcia and J. C. Osborn, *Nucl. Phys.* **A770**, 141 (2006).
- [15] A. M. Garcia-Garcia and J. C. Osborn, *Phys. Rev. D* **75**, 034503 (2007).
- [16] T. G. Kovacs, *Phys. Rev. Lett.* **104**, 031601 (2010).
- [17] T. G. Kovacs and F. Pittler, *Phys. Rev. Lett.* **105**, 192001 (2010).
- [18] R. V. Gavai, S. Gupta, and R. Lacaze, *Phys. Rev. D* **77**, 114506 (2008); V. G. Bornyakov, E. V. Luschevskaya, S. M. Morozov, M. I. Polikarpov, E.-M. Ilgenfritz, and M. Muller-Preussker, *Phys. Rev. D* **79**, 054505 (2009).
- [19] P. de Forcrand, *AIP Conf. Proc.* **892**, 29 (2007).
- [20] Y. Aoki, Z. Fodor, S. D. Katz, and K. K. Szabo, *J. High Energy Phys.* **01** (2006) 089.
- [21] S. Borsanyi, G. Endrodi, Z. Fodor, A. Jakovac, S. D. Katz, S. Krieg, C. Ratti, and K. K. Szabo, *J. High Energy Phys.* **11** (2010) 077.
- [22] F. Siringo and G. Piccitto, *J. Phys. A* **31**, 5981 (1998).
- [23] F. Wegner, *Z. Phys. B* **36**, 209 (1980).
- [24] C. Aubin, C. Bernard, C. DeTar, J. Osborn, S. Gottlieb, E. Gregory, D. Toussaint, U. Heller, J. Hetrick, and R. Sugar (MILC Collaboration), *Phys. Rev. D* **70**, 114501 (2004).
- [25] L. Del Debbio, L. Giusti, M. Luscher, R. Petronzio, and N. Tantalò, *J. High Energy Phys.* **02** (2006) 011.
- [26] L. Giusti and M. Luscher, *J. High Energy Phys.* **03** (2009) 013.
- [27] S. Borsanyi, Z. Fodor, C. Hoelbling, S. D. Katz, S. Krieg, C. Ratti, and K. K. Szabó (Wuppertal-Budapest Collaboration), *J. High Energy Phys.* **09** (2010) 073.
- [28] A. Bazavov, T. Bhattacharya, M. Cheng, C. DeTar, H. T. Ding, S. Gottlieb, R. Gupta, P. Hegde *et al.*, *Phys. Rev. D* **85**, 054503 (2012).
- [29] T. G. Kovacs and F. Pittler, *Proc. Sci., LATTICE2011* (2011) 213 [[arXiv:1111.3524](https://arxiv.org/abs/1111.3524)].
- [30] A. M. Halasz, T. Kalkreuter, and J. J. M. Verbaarschot, *Nucl. Phys. B, Proc. Suppl.* **53**, 266 (1997).
- [31] F. Bruckmann, T. G. Kovacs, and S. Schierenberg, *Phys. Rev. D* **84**, 034505 (2011).
- [32] M. Cheng, S. Datta, A. Francis, J. van der Heide, C. Jung, O. Kaczmarek, F. Karsch, E. Laermann *et al.*, *Eur. Phys. J. C* **71**, 1564 (2011).
- [33] Y. V. Fyodorov and A. D. Mirlin, *Phys. Rev. B* **51**, 13403 (1995); F. Evers and A. D. Mirlin, *Phys. Rev. Lett.* **84**, 3690 (2000); A. Mildemberger, F. Evers, and A. D. Mirlin, *Phys. Rev. B* **66**, 033109 (2002); A. D. Mirlin and F. Evers, *Phys. Rev. B* **62**, 7920 (2000).
- [34] S. Schierenberg, F. Bruckmann, and T. Wettig, *Phys. Rev. E* **85**, 061130 (2012).
- [35] S. M. Nishigaki, [arXiv:1208.3878](https://arxiv.org/abs/1208.3878) [*Prog. Theor. Phys.* (to be published)]; *Phys. Rev. D* **86**, 114505 (2012).
- [36] S. M. Nishigaki, *Phys. Rev. E* **58**, R6915 (1998); **59**, 2853 (1999).
- [37] M. M. Anber, E. Poppitz, and M. Unsal, *J. High Energy Phys.* **04** (2012) 040; M. Unsal, *Phys. Rev. D* **86**, 105012 (2012); E. Poppitz, T. Schaefer, and M. Unsal, *J. High Energy Phys.* **10** (2012) 115.